Optical gaps and excitons in semiconducting transition metal carbides (MXenes)

Electronic Supplementary Information

Tomi Ketolainen and František Karlický‡
Department of Physics, Faculty of Science, University of Ostrava, 30. dubna 22, 701 03 Ostrava, Czech Republic

The absorbance spectra computed with the PBE functional, HSE06 hybrid functional, and TD-HSE06 method for Sc_2CF_2 and Ti_2CO_2 are presented in Figs. S1 and S2, respectively.

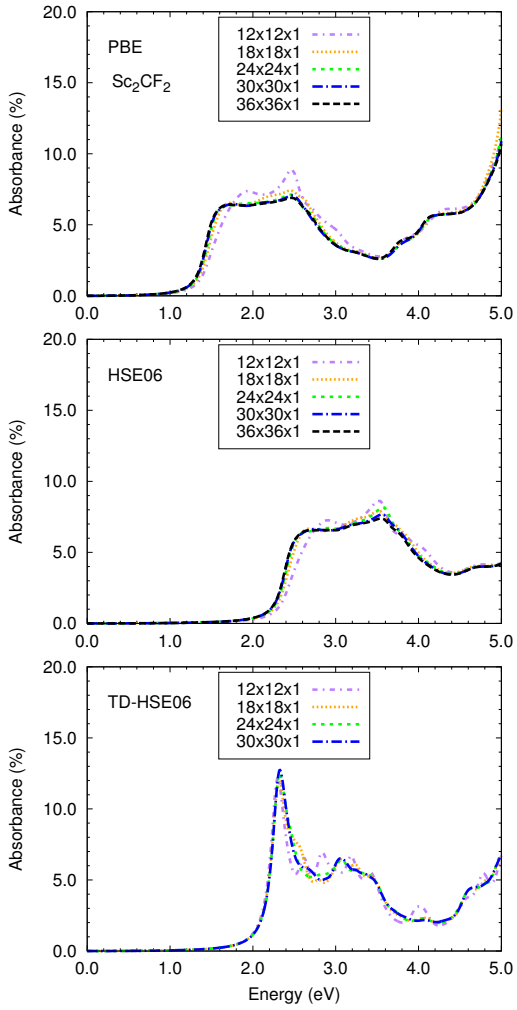

Figure S1. Optical absorbance spectra determined using different methods and k-point grids for Sc_2CF_2.

Calculating the absorbance spectra with several k-point grids shows that the PBE and HSE06 curves converge rapidly between 0.0 and 5.0 eV. In contrast, some oscillations can be seen in the TD-HSE06 spectrum curves particularly in the case of Ti_2CO_2 but the first excitation energies are quite well converged with the $24 \times 24 \times 1$ k-point grid, which can be observed in Fig. S2.

‡ frantisek.karlicky@osu.cz

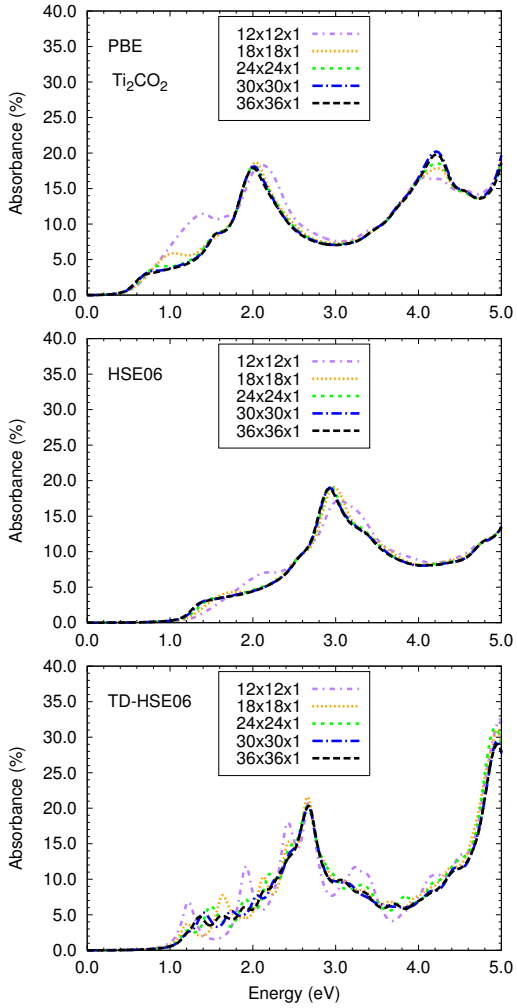

Figure S2. Optical absorbance spectra determined using different methods and k-point grids for Ti_2CO_2.

TABLE S1. The numbers of occupied (Occ.) and virtual (Virt.) bands, included in the Casida calculations (TD-HSE06). Reliability of optical absorbance spectra is ensured for photon energies up to 5 eV (see also Figure S4).

M_2CT_2 MXene	Occ.	Virt.
Sc_2CF_2	3	9
$Sc_2C(OH)_2$	7	8
Ti_2C	5	11
Ti_2CO_2	8	11
Cr_2CF_2	5	5
$Cr_2C(OH)_2$	8	10
Mn_2CO_2 (AFM)	4	7
Mn_2CO_2 (FM)	10	8

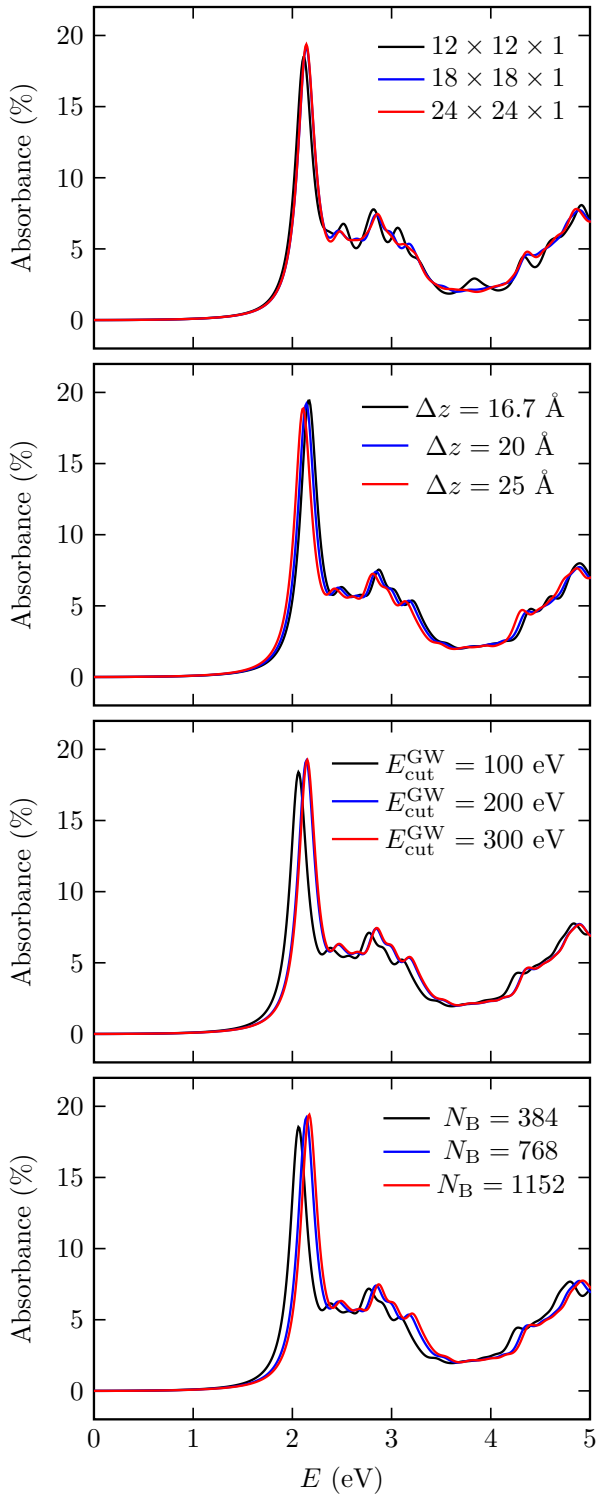

Figure S3. Convergence properties of optical absorbance A (A_{xx} component) for Sc_2CF_2 computed with G_0W_0+BSE method: (top) dependence on the k-point grid, (middle top) dependence on the vacuum space Δz, (middle bottom) dependence on the GW energy cut-off $E_{\text{cut}}^{\text{GW}}$, and (bottom) dependence on the number of considered bands N_{B} in an input DFT calculation. Our standard G_0W_0+BSE calculation parameters are: the number of bands is $N_{\text{B}} = 768$ (24 of them updated in GW and, finally 3 occupied and 9 virtual states in BSE), plane-wave energy cut-off $E_{\text{cut}} = 500$ eV, GW cut-off $E_{\text{cut}}^{\text{GW}} = 200$ eV, $\Delta z = 20$ Å, and 18×18×1 k-point grid. Each subplot is the change in just one mentioned parameter. This setup leads to a direct quasiparticle gap of $E_{\text{gap}}^{\text{GW}} = 2.82$ eV and optical gap of $E_{\text{exc}}^{\text{BSE}} = 2.14$ eV.

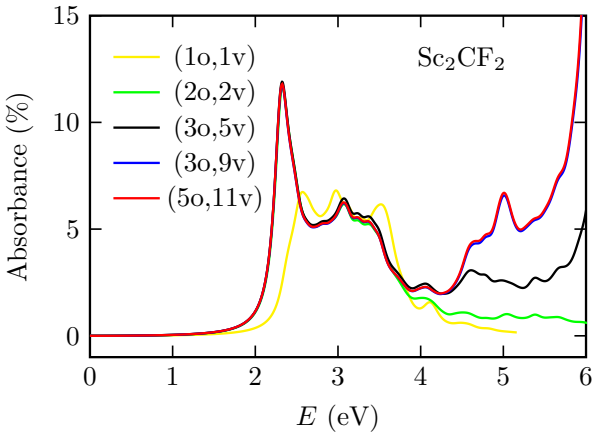

Figure S4. Dependence of optical absorbance for Sc_2CF_2 computed with the TD-HSE06 method on the number of considered bands in the final (TD) step (o=occupied, v=virtual). Our final choice was always given by a criterion to have reliable optical absorbance spectra for photon energies up to 5 eV (here 3o and 9v was sufficient, see Table S1 for other materials).

TABLE S2. HSE06 band energies (eV) at the Γ-point of Cr_2CF_2 (AFM) around the Fermi energy and the occupation numbers. The results are presented for both spin states (up and down). Here we report 5 occupied and 5 unoccupied bands as relevant (and used for a subsequent TD-HSE06 calculation) for Figure 6c of the main text. The band values are almost identical (maximal difference of 0.000001 eV), and the similar is valid for all k-points included in calculations.

Band no.	Energy (up)	Energy (down)	Occ. (up)	Occ. (down)
11	-2.667982	-2.667981	1.000000	1.000000
12	-2.667982	-2.667981	1.000000	1.000000
13	-1.586865	-1.586865	1.000000	1.000000
14	-1.586865	-1.586865	1.000000	1.000000
15	-0.563370	-0.563370	1.000000	1.000000
16	1.301336	1.301336	0.000000	0.000000
17	1.462630	1.462629	0.000000	0.000000
18	2.388492	2.388492	0.000000	0.000000
19	2.865924	2.865924	0.000000	0.000000
20	2.865924	2.865924	0.000000	0.000000

TABLE S3. HSE06 band energies (eV) at the Γ-point of Mn_2CO_2 (AFM) around the Fermi energy and the occupation numbers. The results are presented for both spin states (up and down). Here we report 4 occupied and 7 unoccupied bands as relevant (and used for subsequent TD-HSE06 calculation) for Figure 6d of the main text. The band values are almost identical (maximal difference of 0.000001 eV), and the similar is valid for all k-points included in calculations.

Band no.	Energy (up)	Energy (down)	Occ. (up)	Occ. (down)
12	-6.016402	-6.016403	1.000000	1.000000
13	-4.653811	-4.653811	1.000000	1.000000
14	-4.454214	-4.454215	1.000000	1.000000
15	-4.454214	-4.454214	1.000000	1.000000
16	-1.945553	-1.945553	0.000000	0.000000
17	-1.945553	-1.945553	0.000000	0.000000
18	-1.420894	-1.420894	0.000000	0.000000
19	-1.420894	-1.420894	0.000000	0.000000
20	-0.299977	-0.299977	0.000000	0.000000
21	2.421854	2.421854	0.000000	0.000000
22	2.421854	2.421855	0.000000	0.000000

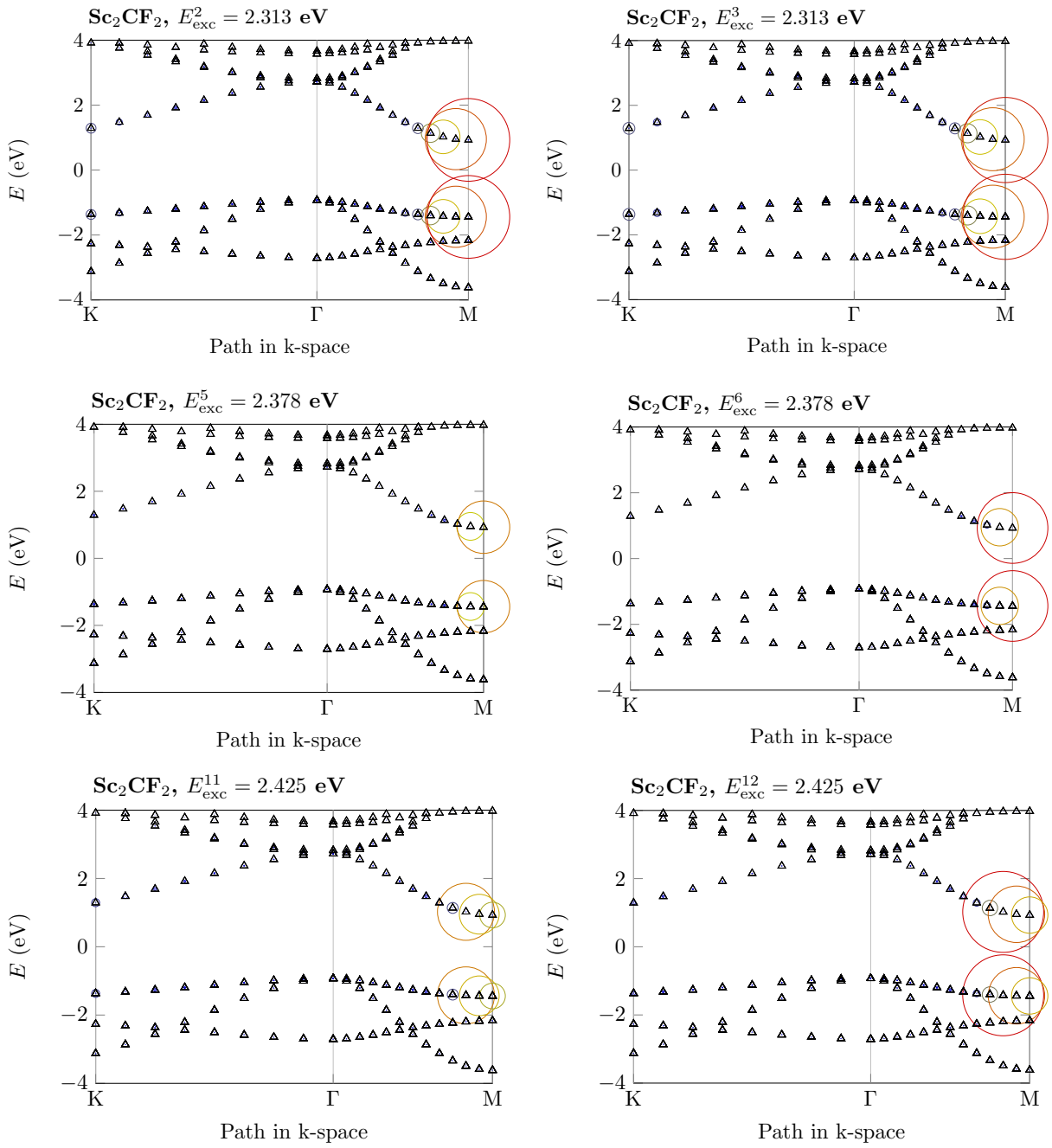

Figure S5. Comparison of important regions in the Brillouin zone of Sc_2CF_2 using the $A^S_{vc\mathbf{k}}$ coefficients (see also Eq. (3) in the main text) for selected excitations $S = 2$, 3 (top), 5, 6, 11, and 12 (bottom). The $|A^S_{vc\mathbf{k}}|$ coefficients (represented by the radii of coloured circles; red = maximum, yellow = middle, grey = minimum) are depicted together with the HSE06 band structure (black triangles). The Fermi energy is set to zero.

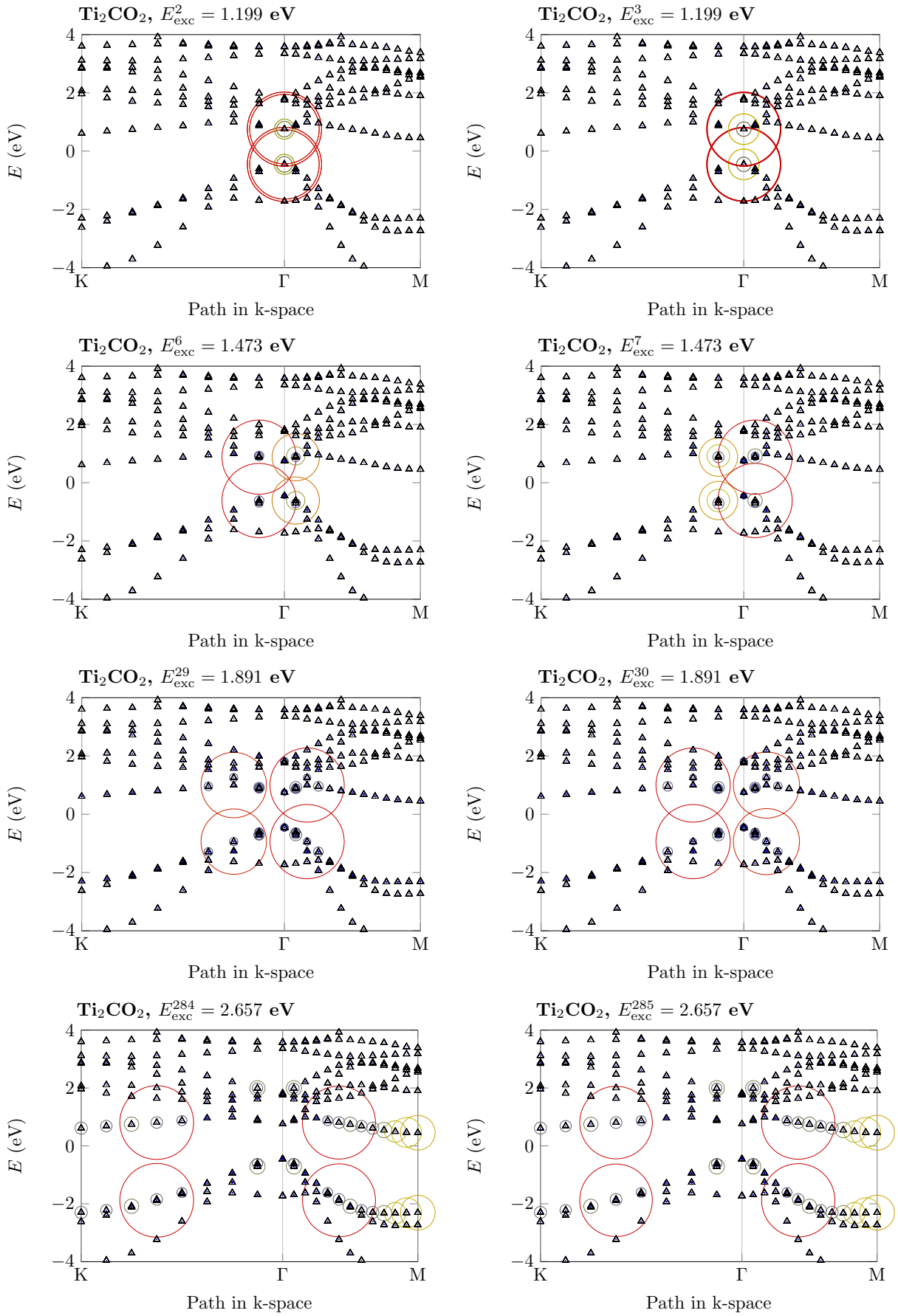

Figure S6. Comparison of important regions in the Brillouin zone of Ti_2CO_2 using the $A^S_{vc\mathbf{k}}$ coefficients (see also Eq. (3) in the main text) for selected excitations $S = 2$, 3 (top), 6, 7, 29, 30, 284, and 285 (bottom). The $|A^S_{vc\mathbf{k}}|$ coefficients (represented by the radii of coloured circles; red = maximum, yellow = middle, grey = minimum) are depicted together with the HSE06 band structure (black triangles). The Fermi energy is set to zero.

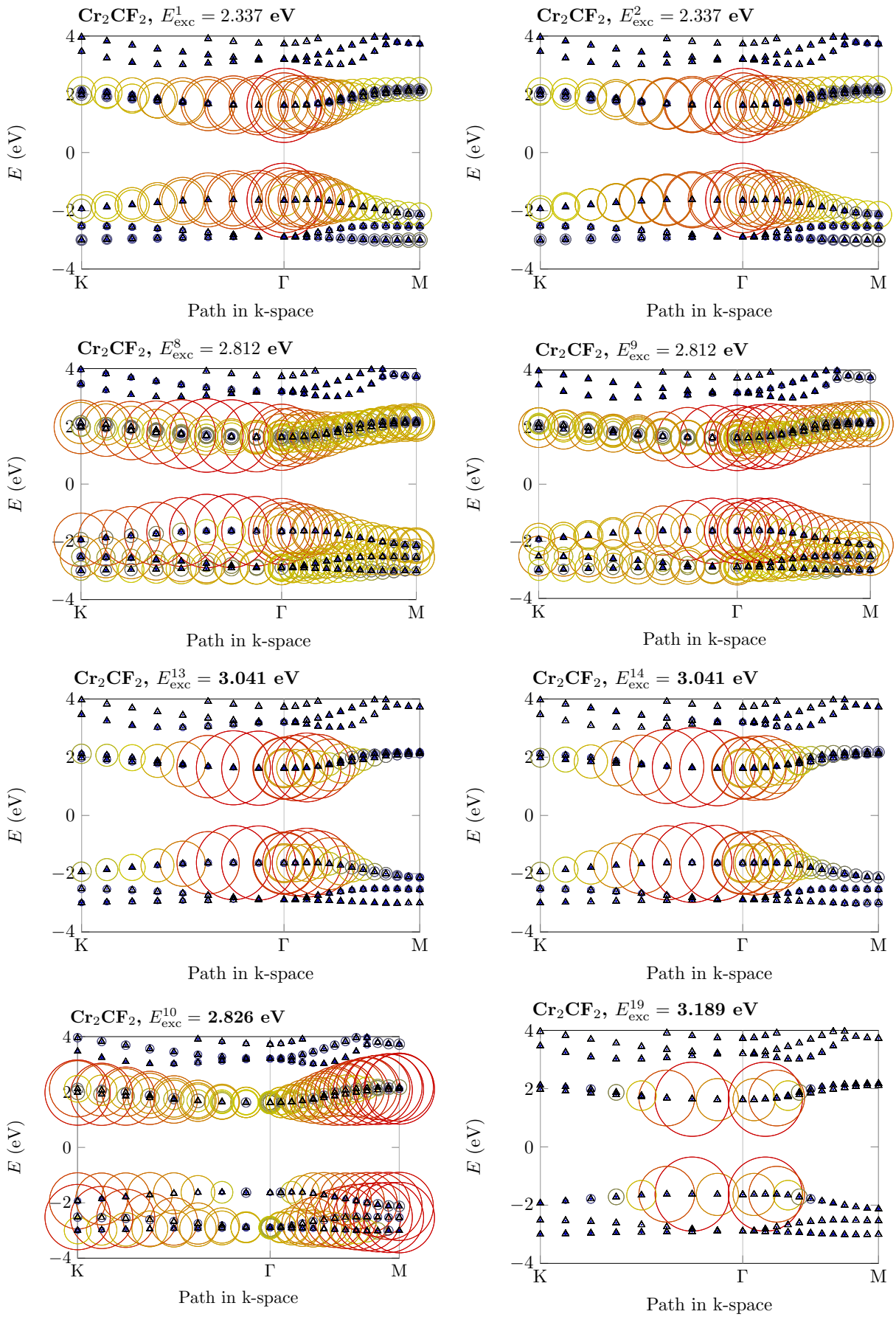

Figure S7. Comparison of important regions in the Brillouin zone of Cr_2CF_2 using the $A^S_{vc\mathbf{k}}$ coefficients (see also Eq. (3) in the main text) for selected excitations $S = 1$, 2 (top), 8, 9, 13, 14, 10, and 19 (bottom). The $|A^S_{vc\mathbf{k}}|$ coefficients (represented by the radii of coloured circles; red = maximum, yellow = middle, grey = minimum) are depicted together with the HSE06 band structure (black triangles). The Fermi energy is set to zero.

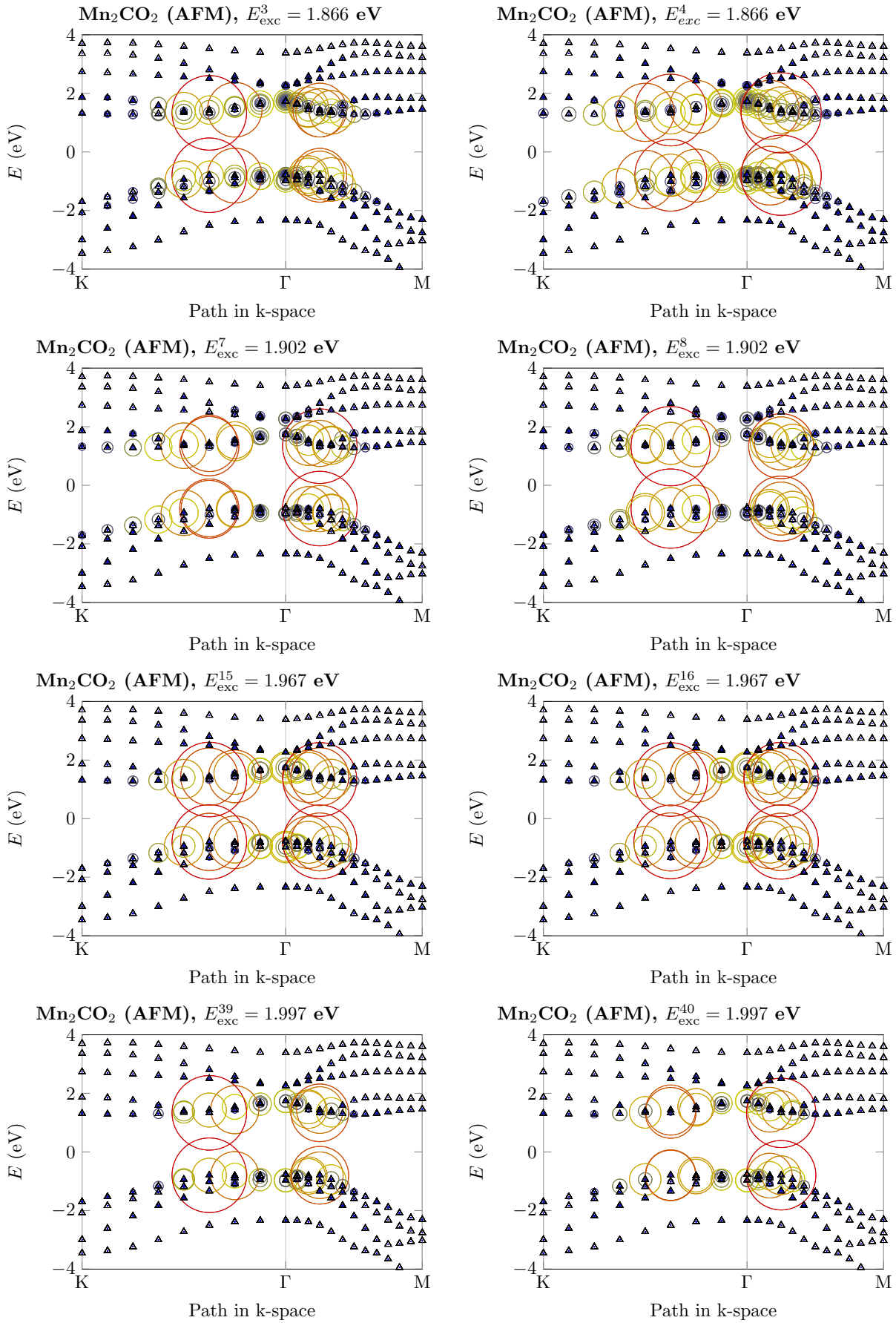

Figure S8. Comparison of important regions in the Brillouin zone of Mn_2CO_2 (AFM) using the $A^S_{vc\mathbf{k}}$ coefficients (see also Eq. (3) in the main text) for selected excitations $S = 3$, 4 (top), 7, 8, 15, 16, 39, and 40 (bottom). The $|A^S_{vc\mathbf{k}}|$ coefficients (represented by the radii of coloured circles; red = maximum, yellow = middle, grey = minimum) are depicted together with the HSE06 band structure (black triangles). The Fermi energy is set to zero.

TABLE S4. Atomic charges (in e) in considered materials provided by Bader charge analysis and using the PBE functional. Values are rounded-off to the two decimal places.

M_2CT_2 MXene	M	C	T	
Sc_2CF_2	1.62	-1.79	-0.73	
$Sc_2C(OH)_2$	1.60	-1.80	-1.25	0.54
Ti_2C	0.96	-1.92		
Ti_2CO_2	1.73	-1.49	-0.98	
Cr_2CF_2	1.36	-1.36	-0.68	
$Cr_2C(OH)_2$	1.32	-1.35	-1.21	0.66
Mn_2CO_2 (AFM)	1.43	-1.16	-0.86	
Mn_2CO_2 (FM)	1.47	-1.19	-0.87	